FOREX Publication
Open Access | Rapid and quality publishing

International Journal of
Electrical and Electronics Research (IJEER)
Research Article | Volume 11, Issue 1 | Pages 192-201 | e-ISSN: 2347-470X

Grid-Tied Solar Power Sharing with V2G and G2V Power Exchange with Dual Bridge Integrated Electrical Vehicle

Ramesh Jatoth[1*] and B. Mangu[2]
[1]*Department of Electrical Engg., University College of Engineering, Osmania University Hyderabad, India, ramesh.jatoth@gmail.com*
[2]*Department of Electrical Engg., University College of Engineering, Osmania University Hyderabad, India, bmanguou@gmail.com*

***Correspondence:** Ramesh Jatoth; ramesh.jatoth@gmail.com

ABSTRACT- An increasing demand of electrical vehicle technology, renewable power is recommended for the charging of vehicle batteries. The proposed electric vehicle battery charging module has the capability of exchanging power between the grid and the vehicle. For this exchange of power, a DAFB circuit is integrated between the battery and the grid. The grid is induced with a solar-powered plant with multiple PV panels generating high power. This renewable power is either utilized by DAFB charging circuit or injected into the grid. The electric vehicle module V2G and G2V conditions are controlled with the PSM technique applied on DAFB with modeling done in MATLAB Simulink environment. The graphs are plotted with time as a reference for different operating conditions. The outcome of this paper is to analyze the DAFB circuit with different operating conditions shifting from charging and discharging modes of the vehicle battery.

Keywords: DAFB (Dual Active Full Bridge), G2V (Grid to Vehicle), PSM (Phase Shift Modulation), MATLAB (Matrix Laboratory), V2G (Vehicle to Grid).

ARTICLE INFORMATION

Author(s): Ramesh Jatoth and B. Mangu;
Received: 26/01/2023; **Accepted**: 06/03/2023; **Published**: 30/03/2023;
e-ISSN: 2347-470X;
Paper Id: IJEER2601-01;
Citation: 10.37391/IJEER.110127
Webpage-link:
www.ijeer.forexjournal.co.in/archive/volume-11/ijeer-110127.html

Publisher's Note: FOREX Publication stays neutral with regard to Jurisdictional claims in Published maps and institutional affiliations.

1. INTRODUCTION

In recent times high pollution affecting the environment causing global warming may create inhabitable conditions for living organisms on the planet. This heavy pollution is caused by different sources which majorly include thermal power plants which are used for electrical power generation [1]. Heavy industrial plants which are operated to manufacture goods and commercial internal combustion vehicles for transportation also generate heavy pollution damaging the environment. From these sources of pollution, heavy industries cannot be stopped or replaced but thermal power plants can be replaced with renewable energy plants. These renewable energy plants may include solar plants, wind farms, biogas plants, and tidal energy plants which generate power using natural sources like solar irradiation, wind speeds, bio waste, and tidal waves [2].

Commercial internal combustion vehicles can be replaced by electrical vehicles which run on battery sources [3]. The battery of the vehicle is charged through a charging circuit connected to the grid and the grid is interconnected with a renewable source PV (Photo-Voltaic) plant [4]. The PV plant module is included with solar panels for DC power generation, a booster converter for DC voltage stabilization, a 3-ph inverter for DC-AC conversion, and an LC filter for harmonic reduction. This PV module is interconnected to the grid and an SRF (Synchronous Reference Frame) controller is integrated to operate a 3-ph inverter in synchronization with the grid voltages. The electric vehicle charging circuit is a DAFB (Dual Active Full Bridge) module which has two bridges with each bridge inclusive of 4-IGBT (Insulated Gate Bipolar Transistor) switches [5]. This DAFB circuit is connected to a 3-ph VSC (Voltage Source Converter) which can convert 3-ph AC to DC and DC to 3-Ph AC. The VSC operates as both a rectifier and also inverter as per the requirement.

For the G2V (Grid to Vehicle) operating state, the VSC operates as a rectifier and for V2G (Vehicle to Grid) operating state the VSC operates as an inverter [6]. In G2V operating state the battery of the vehicle is charged and in V2G operating state the battery of the vehicle is discharged [7]. The complete test system with PV module integration to the grid with DAFB electric vehicle charging circuit is shown in *figure 1*.

FOREX Publication
Open Access | Rapid and quality publishing
International Journal of Electrical and Electronics Research (IJEER)
Research Article | Volume 11, Issue 1 | Pages 192-201 | e-ISSN: 2347-470X

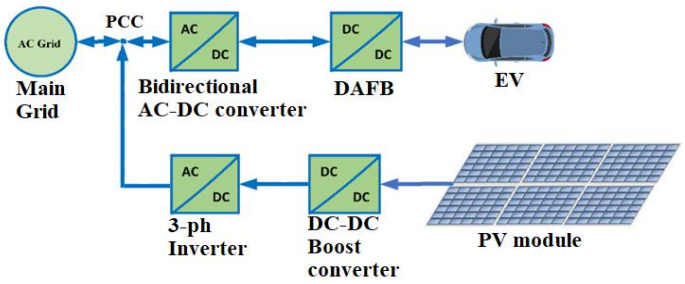

Figure 1: Proposed test system

In the above test system, the PV module boost converter is operated with MPPT (Maximum Power Point Tracking) for maximum power extraction. A β-MPPT algorithm is proposed for a faster response to the changes in the operating conditions of the PV array [8]. The isolated bidirectional DC-DC converter which is DAFB operated with the PSM technique. This paper is included with an introduction to the proposed test system in *section 1* and the PV module configuration is discussed in *section 2*. *Section 3* is included with the working principle of DAFB and both V2G and G2V conditions are discussed. The complete system simulation results with different operating conditions with graphical representation done using MATLAB software are given in *section 4*. In the final *section 5* conclusion to the paper finalizing results and references used for modeling the test system are given.

2. PV MODULE CONFIGURATION

PV panel is a renewable source that generates power by absorbing solar irradiation using p-n type silicon doped material. The power generated by the PV panel is purely DC as the electrons only flow in one direction during generation. The density of electrons depends on the intensity of solar irradiation which normally varies from 200W/mt^2 – 1000 W/mt^2 on a normal day. Therefore, the output power of the panel is directly proportional to solar irradiation in a day which varies as per the intensity. Hence the panel voltage needs to be stabilized using external circuit topology and also increase the magnitude as per the requirement. For this, a boost converter is adopted which is controlled using an MPPT controller [8].

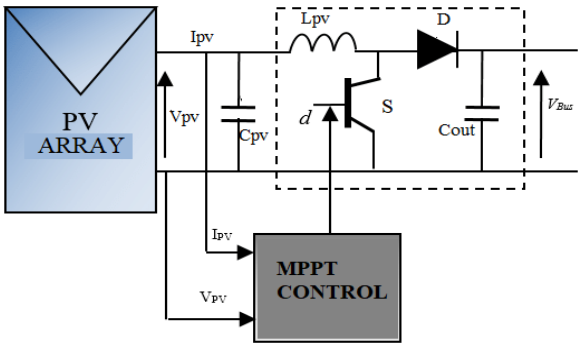

Figure 2: PV module structure

The MPPT controller takes feedback from PV panel voltage and current for estimation of the required duty ratio for maximum power extraction. The connection of multiple panels in parallel or series makes a PV array which is represented as a solar plant. This PV array connected to the booster converter controlled by the MPPT controller circuit structure is shown in *figure 2*.

In the given *figure 2* the passive element C_{pv} is the input capacitance which reduces ripple in PV voltage, L_{pv} is the boosting inductor for energy storage and discharge, S is the switching IGBT controlled by MPPT control, D is the reverse current blocking diode and C_{out} is the output capacitance for mitigating DC bus voltage (V_{bus}) ripple.

2.1 MPPT Control

The ON and OFF time of IGBT is decided by MPPT control which is taking signals of PV array voltage V_{pv} and current I_{pv}. The MPPT control induced in the PV module is β-MPPT which has a faster response and higher power extraction as compared to conventional P&O MPPT control [9]. The β-MPPT algorithm for change in duty ratio (d) as per the change in V_{pv} and I_{pv} can be seen in form of a flow chart in *figure 3*.

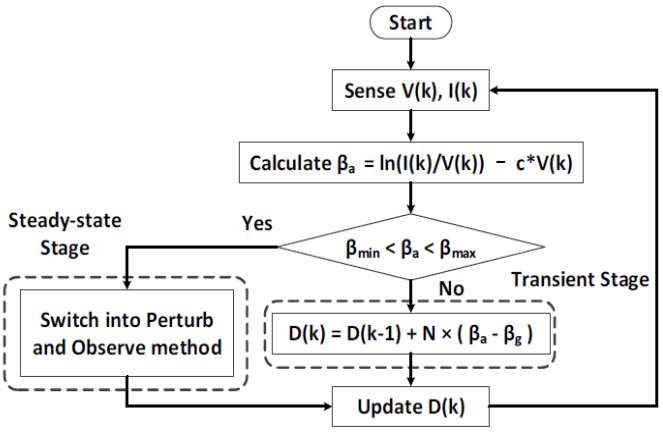

Figure 3: β-MPPT control flow chart

As observed in *figure 3* the flow chart starts with V(k) and I(k) present measurements which represent Vpv and Ipv. [10] An instantaneous β_a value is calculated using these V(k) and I(k) values which is given in *equation (1)*.

$$\beta_a = \ln\left(\frac{I(k)}{V(k)}\right) - c.V(k) \quad (1)$$

In the above *equation (1)* variable 'c' is the diode constant which is given as *equation (2)*.

$$c = \frac{q}{N_S.A.K.T} \quad (2)$$

Here, 'q' is the charge of an electron with a value 1.602 x 10^{-19} C, T is the temperature in Kelvin, K is Boltzmann

FOREX Publication
Open Access | Rapid and quality publishing
International Journal of Electrical and Electronics Research (IJEER)
Research Article | Volume 11, Issue 1 | Pages 192-201 | e-ISSN: 2347-470X

constant with value 1.38 x 10^{-23} J/K and A is the diode ideal factor taken as 0.1.

After the calculation of β_a value, it is then compared with minimum and maximum limit values β_{min} and β_{max} respectively [10]. As per the β_a value it is decided that the controller works in transient mode or steady-state mode. Now as per the mode, the duty ratio value is adjusted either it has to change as per P&O (Perturb & Observe) MPPT control or β-MPPT control [11]. The steady-state mode is integrated with P&O MPPT control and the transient mode is integrated with a change in duty ratio given as *equation (3)*.

$$D(k) = D(k-1) + N.(\beta_a - \beta_g) \quad (3)$$

Here, in the above-given equation (3) D(k-1) is the past duty ratio value, N is the scaling factor and β_g is the guiding value which is the mean of β_{max} *and* β_{min} given as *equation (4)*.

$$\beta_g = \frac{(\beta_{max}+\beta_{min})}{2} \quad (4)$$

The values of β_{max} *and* β_{min} are taken as per the stability of β_a value [12]. This updated duty ratio D(k) is compared to a high-frequency saw-tooth waveform generating a pulse for switch S of the boost converter. In steady-state mode, the duty ratio value is adjusted by the P&O MPPT algorithm which is a conventional method used in most of the modules. The response of the complete MPPT control is rapid in a transient state as the MPPT varies the duty ratio value using the β-MPPT algorithm [13]. A simulation comparative analysis is carried out with both P&O MPPT and β-MPPT algorithms in this paper in *section 4*.

2.2 VSC Module

The 6-switch VSC module comprises 6-IGBT switches connected with an anti-parallel diode for each IGBT. The VSC operates as an inverter when the IGBTs are fed with PWM (Pulse width modulation) pulses generated using the SRF control structure. This VSC module with SRF controller is integrated for both the PV module and DAFB circuit (vehicle battery module) [14]. For the PV module, the VSC only operates as an inverter whereas, for the DAFB module, it operates as a rectifier as well as an inverter. During the rectification of VSC implementing G2V condition for charging the battery, pulses to the VSC are removed making the body diodes of all the 6-IGBTs work as a 3-ph diode bridge rectifier [14].

During V2G condition for discharging the battery and for sharing of PV power through the VSC to the grid SRF control is used with feedback from the PCC (point of common coupling) [15]. 3-ph voltages and currents at the PCC are considered for the generation of pulses to VSC with synchronization to the grid. The complete structure of SRF control is shown in *figure 4*.

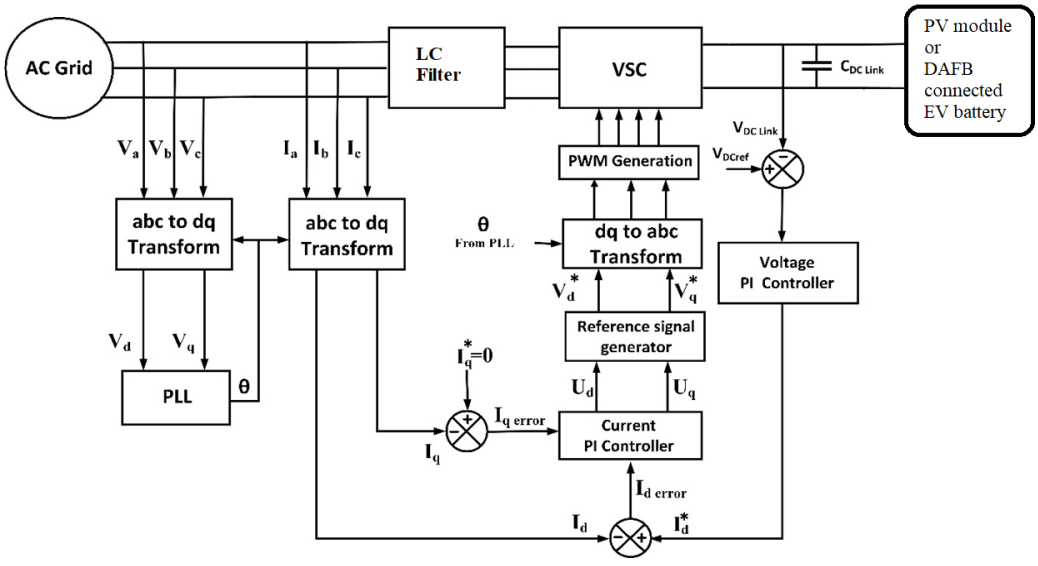

Figure 4: Overall controlled diagram for the proposed system

Initially, the 3-ph voltages and currents are converted to *dq*-axis components by Park's transformation given as *equation (5).*

$$\begin{bmatrix} F_d \\ F_q \\ F_0 \end{bmatrix} = \begin{bmatrix} Sin\,\theta & -Cos\,\theta & 0 \\ Cos\,\theta & Sin\,\theta & 0 \\ 0 & 0 & 1 \end{bmatrix} \begin{bmatrix} F_a \\ F_b \\ F_c \end{bmatrix} \quad (5)$$

In the given *equation (5)* the F can be either voltage or current and θ is the angle of phase A of the grid calculated by PLL (Phase Locked Loop) [16]. The I_d-I_q measured components are compared to reference current components I_d*-I_q* generating I_d –I_q error signals. Here the I_q* component is taken as '0'

FOREX Publication
Open Access | Rapid and quality publishing
International Journal of Electrical and Electronics Research (IJEER)
Research Article | Volume 11, Issue 1 | Pages 192-201 | e-ISSN: 2347-470X

considering no exchange of reactive power from VSC. [16] The I_d* is calculated by a DC voltage regulator (PI) fed with a DC voltage error signal which is given as *equation (6)*

$$I_d^* = \left(K_p + \int Ki\right)(V_{DC\,ref} - V_{DC\,link}) \quad (6)$$

In *equation (6)* $V_{DC\,ref}$ is the reference DC voltage and $V_{DC\,link}$ is the measured DC link voltage at the DC link capacitor $C_{DC\,link}$.

These I_d-I_q error signals are fed to the current regulator (PI) for the generation of U_dU_q signals. The final reference signal generator takes input from U_qU_q, IdIq, and V_dV_q components generating a reference signal for the operation of the VSC [17]. The internal structure of the reference signal generator is shown below in *figure 5*.

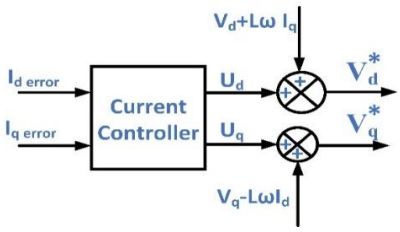

Figure 5: Final Vd*-Vq* generator

The above structure is mathematically represented by *equations (7) and (8).*

$$V_d^* = Ud + Vd + L\omega I_q \quad (7)$$

$$V_q^* = Uq + Vq - L\omega I_d \quad (8)$$

This final reference voltage signals V_d*-V_q* is converted to 'abc' components which are the reference signals for SPWM (Sinusoidal PWM) technique [17]. The inverse Park's transformation is given as *equation (9).*

$$\begin{bmatrix} V_a \\ V_b \\ V_c \end{bmatrix} = \begin{bmatrix} Sin\,\theta & Cos\,\theta & 1 \\ Sin\left(\theta - \frac{2\pi}{3}\right) & Cos\left(\theta - \frac{2\pi}{3}\right) & 1 \\ Sin\left(\theta + \frac{2\pi}{3}\right) & Cos\left(\theta + \frac{2\pi}{3}\right) & 1 \end{bmatrix} \begin{bmatrix} V_d^* \\ V_q^* \\ V_0^* \end{bmatrix} \quad (9)$$

Here, V_0^* is considered as '0' as there is no biasing of voltage signals.

3. DAFB CIRCUIT WORKING PRINCIPLE

In the electric vehicle module DAFB circuit is considered for bidirectional power flow, charging, and discharging of the electric vehicle battery [17]. The DAFB circuit comprises two full bridges with IGBT switches connected in a two-legged format. Both the full bridges are magnetically coupled and electrically isolated and connected with a high-frequency transformer (HFTF) [18]. The primary side connected full-bridge operates as an inverter at a very high frequency in the range of 20kHz-50kHz. The secondary side connected full-bridge operates as a rectifier which also operates at the same frequency as that of the primary side full bridge.

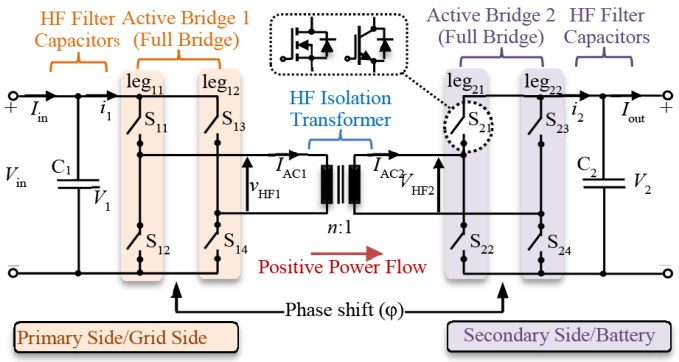

Figure 6: DAFB circuit topology

Primary side full bridge DC terminals are connected to 3-ph VSC which operates as a rectifier during charging mode and as an inverter during discharging mode. The secondary side full bridge DC terminals are connected to an electric vehicle battery. Both the full bridges are operated with the same switching frequency and fixed duty ratio of 50% [19] [20]. To control the direction of power flow (V2G or G2V) phase shift modulation technique is adopted for the DAFB module [21]. For charging mode which is G2V condition, the secondary full bridge is operated with a phase delay with a specific lagging phase shift angle (φ). And for discharging mode which is V2G condition the primary full bridge is operated with a phase delay with a lagging phase shift angle.

The phase shift angle φ is determined by a feedback loop control with a feedback signal taken from the battery current for current control [21]. The charge and discharge current of the battery is set by a reference value which is set as per the requirement. Below is the control structure of the DAFB circuit topology which controls the phase shift of the full bridges as per the mode of operation.

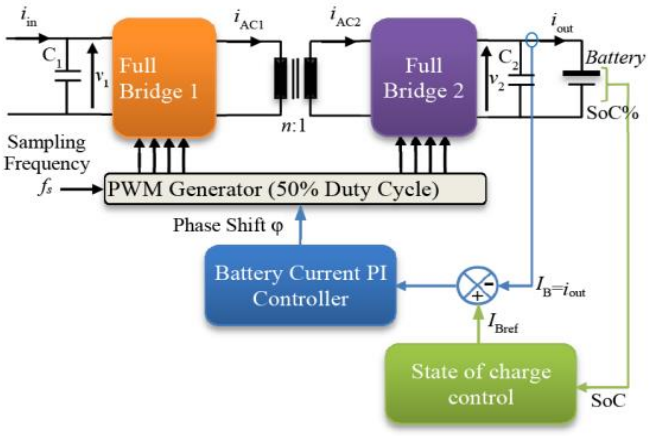

Figure 7: Phase shift controller of DAFB

FOREX Publication
Open Access | Rapid and quality publishing
International Journal of Electrical and Electronics Research (IJEER)
Research Article | Volume 11, Issue 1 | Pages 192-201 | e-ISSN: 2347-470X

As seen the measured battery current I_B is compared to I_{Bref} and the error signal is given to the battery current controller which is a PI controller with specific Kp Ki gain values [22].

A phase shift angle φ is generated by the PI controller which is used for creating delay in the pulses for the full bridge switches. The given DAFB circuit is modeled with an equivalent circuit as given in *figure 8*.

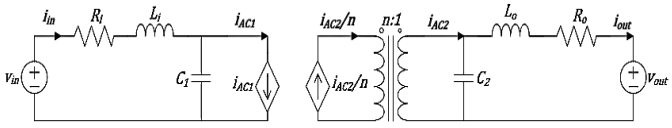

Figure 8: Equivalent diagram of DAFB circuit

Here V_{in} V_{out} and i_{in} i_{out} are the input and output voltages and currents of the DAFB concerning the phase shift created bridge.

The R_i L_i C_1 are the passive components of the primary side winding and R_o L_o C_2 are the secondary side winding passive components. The current of the primary winding is given as i_{AC1} inducing current to secondary side i_{AC2}/n concerning transformer ratio. (n:1).

The passive components are determined as per the input currents of the DAFB module which are given as

$$C_1 \frac{dV_1}{dt} = i_{in} - i_{AC1} \quad (10)$$

$$L_i \frac{di_{in}}{dt} + R_i i_{in} = V_{in} - V_1 \quad (11)$$

$$C_2 \frac{dV_2}{dt} = i_{AC2} - i_{out} \quad (12)$$

$$L_o \frac{di_{out}}{dt} + R_o i_{out} = V_2 - V_{out} \quad (13)$$

Here, V_1 and V_2 are the voltages across the capacitive elements C_1 and C_2 respectively. The primary and secondary currents of the transformer are determined as

$$i_{AC1} = \frac{V_1+nV_2}{R} d + \frac{V_1-nV_2}{R}(1-d) + \frac{L}{RT}\left(I_1 + \frac{V_1+nV_2}{R}\right)\left(e^{-\left(\frac{R}{L}\right)dT} - 1\right) + \frac{L}{RT}\left(\frac{V_1-nV_2}{R} - I_2\right)\left(e^{-\left(\frac{R}{L}\right)(T-dT)} - 1\right) \quad (14)$$

$$i_{AC2} = -\frac{nV_1+n^2V_2}{R} d + \frac{nV_1-n^2V_2}{nR}(1-d) - \frac{L}{RT}\left(nI_1 + \frac{nV_1+n^2V_2}{R}\right)\left(e^{-\left(\frac{R}{L}\right)dT} - 1\right) + \frac{L}{RT}\left(\frac{nV_1-n^2V_2}{R} - nI_2\right)\left(e^{-\left(\frac{R}{L}\right)(T-dT)} - 1\right) \quad (15)$$

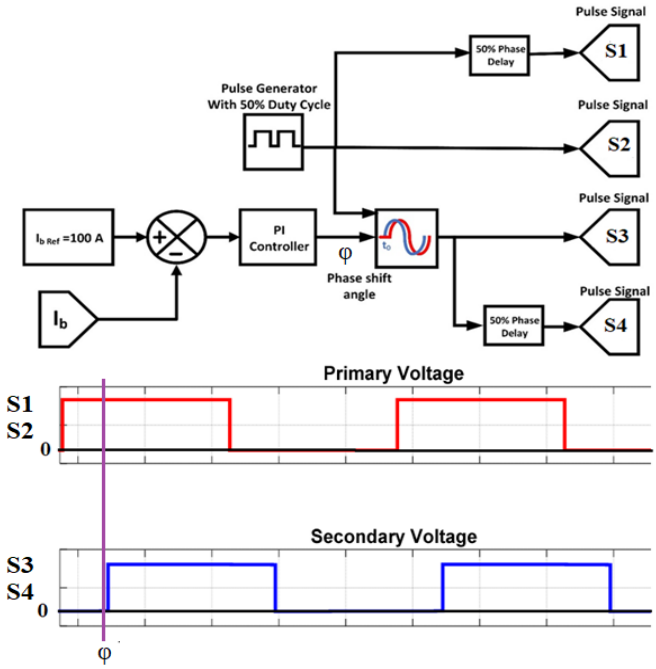

Figure 9: Phase shift angle internal control

The internal structure for the phase shift control can be seen in *figure 9*. As seen in *figure 9* a current reference is compared to the measured battery current and the error is fed to PI which generates phase shift angle φ for the switches S3 and S4. The phase shift is applied to the secondary side full bridge switches for G2V operating conditions. For the V2G operating condition the same controller is used creating phase shift φ for the primary side full bridge switches [23]. The power transfer P_t concerning change in phase angle φ and input-output voltages is given as

$$P_t = \frac{V_i^2}{wL} \cdot \frac{V_o}{N.V_i}\left(1 - \frac{|\varphi|}{\pi}\right) \quad (16)$$

Here, V_i is the input voltage, V_o is the output voltage, N is the transformer turns ratio, φ is the phase shift angle, w is the angular switching frequency given as $w = 2.\pi.f_s$ and L is the leakage inductance.

Different operating conditions of the converter and simulation results of the proposed test system are carried out in the next section with graphs plotted concerning time.

4. RESULTS DISCUSSION

All the modules of the test system which include the Grid system, PV module, and DAFB electric vehicle battery charging circuit are modeled in MATLAB Simulink environment using the 'Power systems' toolbox. The parameters of the test system for the simulation analysis are given in *table 1*.

FOREX Publication
Open Access | Rapid and quality publishing
International Journal of Electrical and Electronics Research (IJEER)
Research Article | Volume 11, Issue 1 | Pages 192-201 | e-ISSN: 2347-470X

Table 1: Test system parameters

Name of the parameter	Values
Grid	100MVA, 11kV, 50Hz
PV module	V_{mp} = 54.7V, I_{mp} = 5.58A, V_{oc} = 64.2V, 5.96A, N_p = 64, N_s = 5, $P_{pv\ opt}$ = 100kW.
Boost converter	R_b = 0.005Ω, L_b = 5mH, C_{out} = 12mF, fsw = 5kHz.
β-MPPT	D_{int} = 0.5, B_{min} = -6500, B_{max} = -5400, B_g = -6000, MPPT gain = 5,
SRF controller	DC regulator gains: Kp = 7, Ki = 800 AC regulator gains: Kp = 0.3, Ki = 20 Vdc ref = 500V, Switching frequency = 1650Hz.
DAFB module	HFTF winding ratio- 1:1, $I_{bat\ ref}$ = 100A, High switching frequency = 20kHz, Phase shift regulator gains: Kp=0.1x10^{-6}, Ki = 5x10^{-9}.
Electric vehicle battery	Type: Lithium Ion, Pnom = 30kWh, Vnom = 320V, Capacity = 94Ah.

With the above parameters, the simulation is modeled first with only the PV module connected to the grid operated by the SRF controller. A comparative analysis is done with P&O-MPPT and β-MPPT to determine the optimal technique. The maximum power extraction from PV array comparison between these two techniques is shown in *figure 10*.

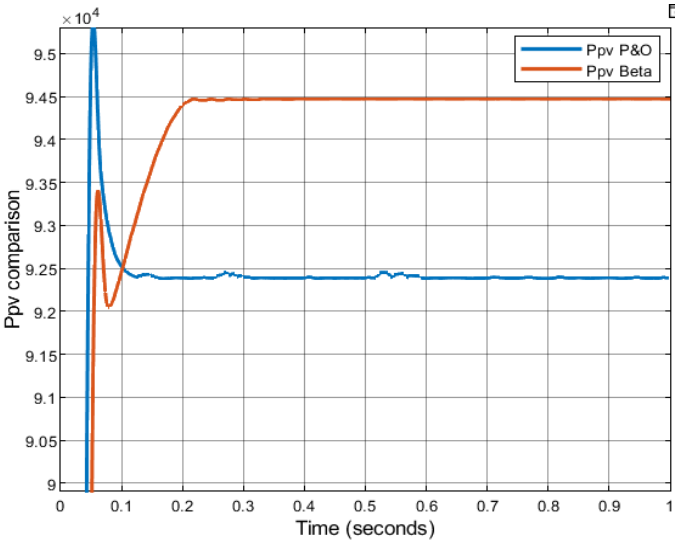

Figure 10: Comparison between P&O-MPPT and β-MPPT total extracted power from PV array

As seen the β-MPPT module power extraction has less initial peak value generation and the extracted power is higher as compared to the P&O-MPPT technique. The DC voltage of the boost converter with both techniques is maintained as 500V as per the given reference value.

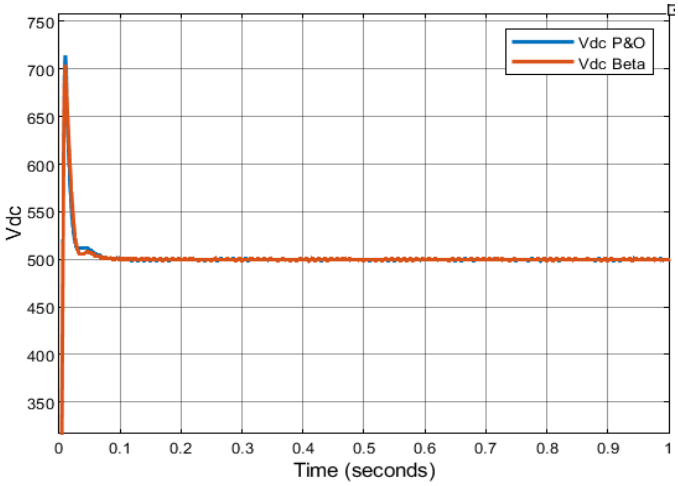

Figure 11: DC link voltage of boost converter of both the MPPT technique test systems

A parametric comparative *table 2* with both MPPT techniques comparison is given.

Table 2: MPPT comparison

MPPT parameter	P&O-MPPT	β-MPPT
$P_{int\ peak}$	96kW	93.5kW
$P_{extracted}$	92.5kW	94.5kW
$V_{dc\ peak}$	710V	700V
V_{dc}	500V	500V

After the extraction from the PV array by the boost converter and boosting the voltage to 500V, the DC power is converted to 3-ph AC by VSC. After the conversion, the power is injected into a 3-ph grid through a step-up transformer (260V/11kV). A comparative graph of injected power by PV module by both the MPPT techniques is given in *figure 12*.

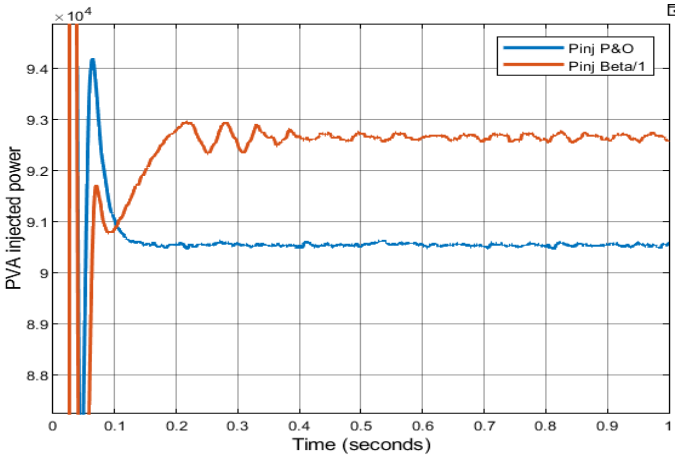

Figure 12: Comparison between P&O-MPPT and β-MPPT injected PV module power to the grid

FOREX Publication
Open Access | Rapid and quality publishing
International Journal of Electrical and Electronics Research (IJEER)
Research Article | Volume 11, Issue 1 | Pages 192-201 | e-ISSN: 2347-470X

As seen the PV module power injection by β-MPPT is high as compared to the P&O-MPPT technique. The power injected by the β-MPPT PV module is recorded at 92.7kW and for P&O-MPPT is 90.5kW. The harmonic analysis of the PV module inverter current using the FFT analysis tool can be seen in *figure 13.*

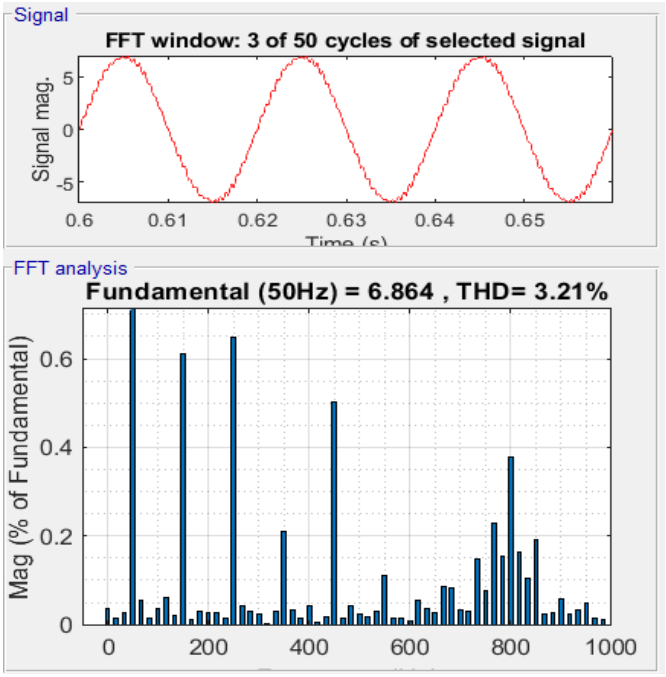

Figure 13: THD of injected PV module current

As seen in *figure 13* the THD (Total Harmonic Distortion) of the source current is at 3.21% which is below 5% as per the IEEE standard benchmark. After optimizing the MPPT controller in the PV module the test system is connected with the DAFB module with VSC controlled as shown in *figure 14.*

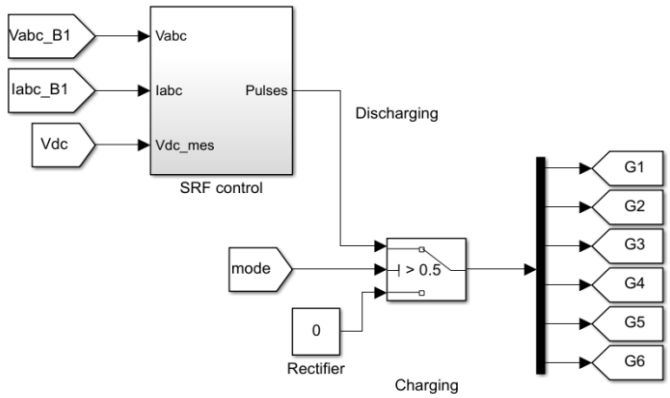

Figure 14: Charge and discharge mode selector of VSC in the DAFB module

As seen the pulses to the VSC in the DAFB module (G1-G6) are selected by a switch block where the selection is done as per the mode of operation. The switching pulses are connected to SRF control making the VSC operate as an inverter when the DAFB module is operating in discharge mode. All the switching pulses are made '0' when the VSC needs to be operated as an uncontrolled rectifier during charge mode. The operating modes of the DAFB module are changed concerning time with a step signal. For signal '0' the DAFB operates in charging mode and for signal '1' DAFB operates in discharging mode. The modes are changed as per the below-given conditions.

***Condition 1*:** Operating in charging mode from 0-0.5sec
***Condition 2*:** Operating in discharging mode from 0.5-1sec

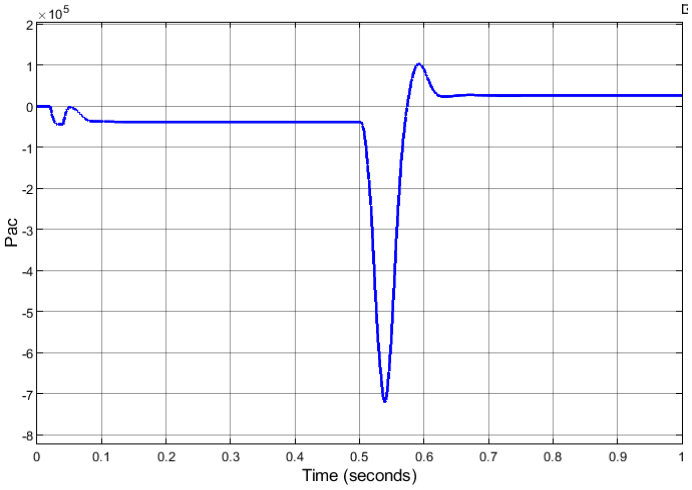

Figure 15: DAFB module AC side active power exchange

The above graph is the power exchange at the PCC between the DAFB module and the grid-connected PV module. Initially, at 0sec the topology is in transient condition and settles at 0.1sec with 38kW of power consumption from the grid by the DAFB module. After 0.5sec the system again goes to a transient state which stabilizes at 0.7sec with 27kW of power injected into the grid from the DAFB module.

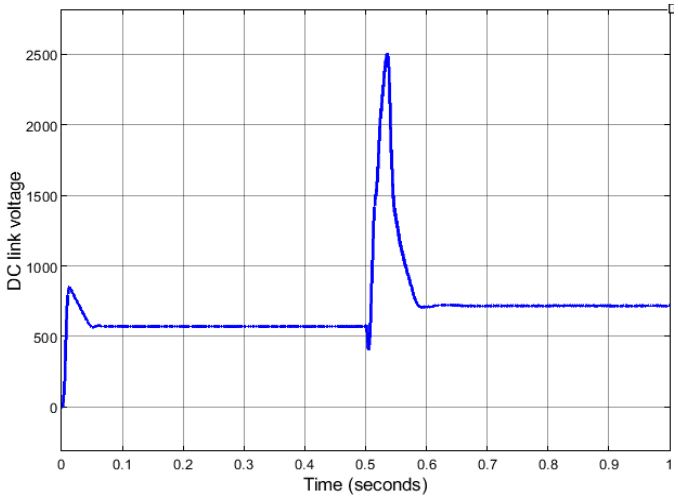

Figure 16: DC link voltage of VSC in DAFB module

FOREX Publication
Open Access | Rapid and quality publishing
International Journal of Electrical and Electronics Research (IJEER)
Research Article | Volume 11, Issue 1 | Pages 192-201 | e-ISSN: 2347-470X

The above *figure 16* is the DC link voltage of the VSC in the DAFB module which maintains at 575V during the charging condition and changes to 700V during discharging condition at 0.5sec.

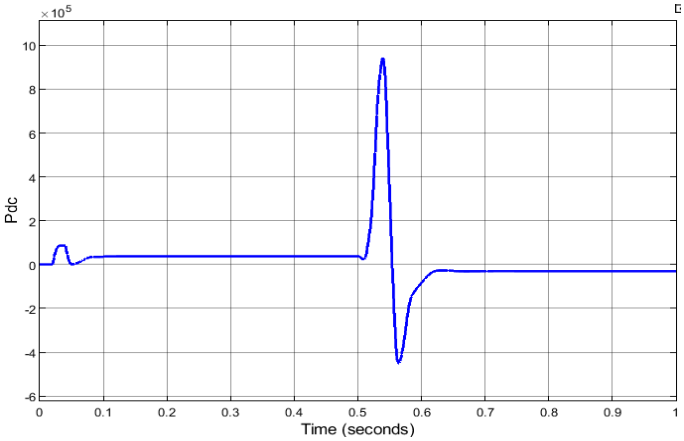

Figure 17: DC power exchange at DC link of VSC in DAFB module

The DC power exchange at the DC link of the VSC can be seen in *figure 17* with a charging power of 38kW and discharging power of 30kW after 0.5sec. From the PV power of 92.7kW 38kW is fed to the DAFB module and the remaining power of 54.7kW is injected into the grid. The final battery power in *figure 18* consumed and discharged from the battery during G2V and V2G conditions is 33kW and 33kW respectively.

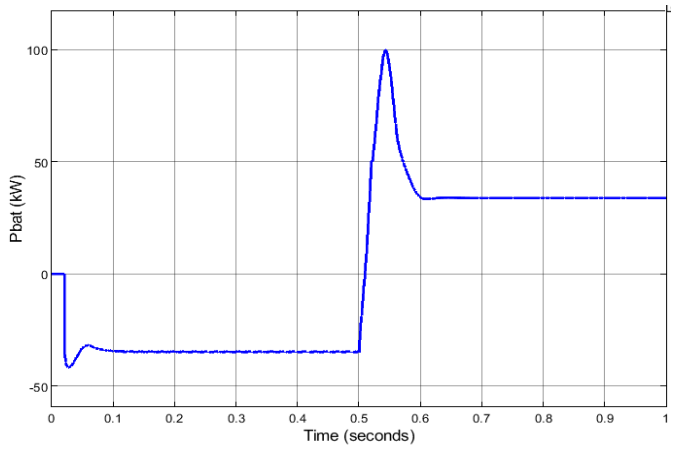

Figure 18: Battery power exchange as per the given condition

In both conditions (G2V and V2G) the reference current is taken the same at 100A. Therefore, the same current magnitude is charged and discharged from the battery by the PSM controlling DAFB. The efficiency of the DAFB module during G2V and V2G conditions is given below.

$$\eta_{G2V} = 100 - \left(\frac{V_{ac}-V_{bat}}{V_{ac}} * 100\right) \ldots\ldots\ldots\ldots \quad (16)$$

$$= 100 - \frac{38kW-33kW}{38kW} = 86.84\%$$

$$\eta_{V2G} = 100 - \left(\frac{V_{bat}-V_{ac}}{V_{bat}} * 100\right) \ldots\ldots\ldots\ldots \quad (17)$$

$$= 100 - \frac{33kW-27kW}{33kW} = 81.81\%$$

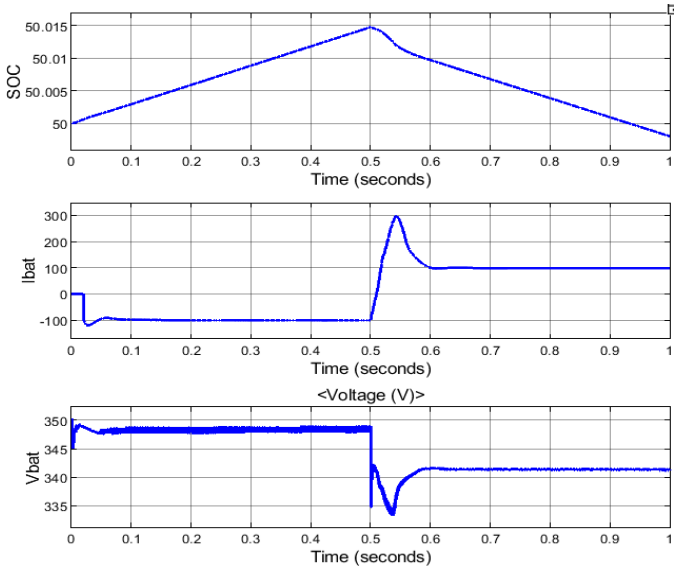

Figure 19: Charge and Discharge battery characteristics of electric vehicle

The above *figure 19* is the battery characteristics which show the State of Charge (SOC), battery current, and Battery voltage. As observed the SOC increases continuously during the charging state (0-0.5sec) and the current reading is shown as -100A representing the charging of the battery. The slope of SOC tends to drop at 0.5sec when the condition is changed to discharge mode. Hence the battery current is shown as +100A representing the discharge of the battery. The battery voltage magnitude moderately fluctuates during the change of operating mode which is normal. The conclusion to the paper with a power comparative analysis table is discussed in the next section.

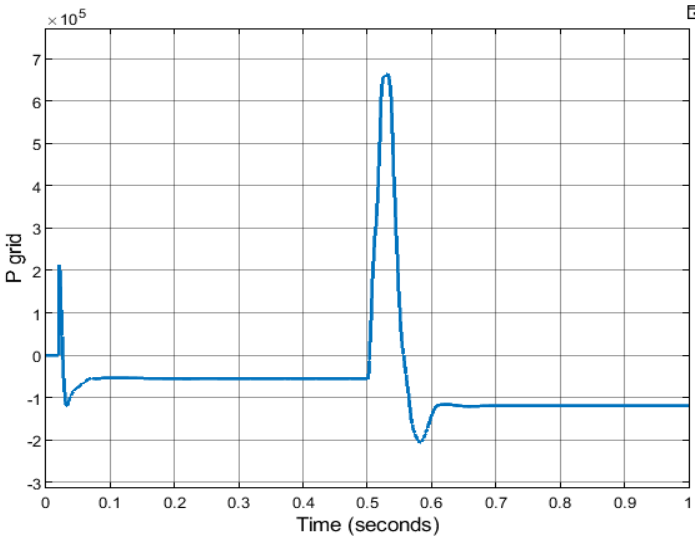

Figure 20: Grid active power

FOREX Publication
Open Access | Rapid and quality publishing
International Journal of Electrical and Electronics Research (IJEER)
Research Article | Volume 11, Issue 1 | Pages 192-201 | e-ISSN: 2347-470X

In above *figure 20* the grid power is shown with the initial value settling at -54.5kW which represents 54.5kW injected into the grid. After the utilization of 38kW power by the DAFB module from 92.5kW power generated by the PV module the remaining power 54.5kW is injected into the grid. At 0.5sec when the DAFB operation is changed to V2G condition the power from the DAFB module 27kW is injected into the grid along with PV module power 92.5kW. Therefore, the total power injected into the grid after 0.5sec is settled at 119.5kW.

5. CONCLUSION

With the given results of the proposed test system, it is determined that the DAFB circuit topology is controlling the G2V and V2G conditions with the PSM technique. For charging the EV battery renewable source PV array is optimally utilized with maximum power extraction using β-MPPT.

A comparative analysis of both the MPPT techniques (P&O and β-MPPT) is done showing 2.2kW more power is extracted from the PV module when β-MPPT is operated. The changes in the battery current directions indicate that the same DAFB circuit can be used as a bidirectional power-sharing module. It is also shown that the efficiency during the G2V and V2G conditions is maintained at around 80% which is acceptable for any power system. The THD of the PV module current is maintained at 3.21% determined by the FFT analysis tool which is below 5% of the IEEE standard.

REFERENCES

[1] D. Pravitasari and S. Nisworo, "New and renewable energy: A review and perspectives," 2017 International Conference on Sustainable Information Engineering and Technology (SIET), 2017.

[2] C. S. Kwok, S. Krishnan, B. H. Tesfagergis and H. Yao Hsu, "Feasibility Study of using Photovoltaic (PV), Wind and Biogas Renewable Energy System in South Australia Household to Maximize the Energy Production from Renewable Sources," 2019 Advances in Science and Engineering Technology International Conferences (ASET), 2019.

[3] M. Ehsani, K. V. Singh, H. O. Bansal and R. T. Mehrjardi, "State of the Art and Trends in Electric and Hybrid Electric Vehicles," in Proceedings of the IEEE, vol. 109, no. 6, pp. 967-984, June 2021.

[4] R. Evode, "Modeling of Electric Grid Behaviors having Electric Vehicle charging stations with G2V and V2G Possibilities," 2021 International Conference on Electrical, Computer, Communications and Mechatronics Engineering (ICECCME), 2021.

[5] C. H. T. Lee, W. Hua, T. Long, C. Jiang and L. V. Iyer, "A Critical Review of Emerging Technologies for Electric and Hybrid Vehicles," in IEEE Open Journal of Vehicular Technology, vol. 2, pp. 471-485, 2021.

[6] B. M. Kumar, A. Kumar, A. H. Bhat and P. Agarwal, "Comparative study of dual active bridge isolated DC to DC converter with single phase shift and dual phase shift control techniques," 2017 Recent Developments in Control, Automation & Power Engineering (RDCAPE), 2017.

[7] S. Bal, D. B. Yelaverthi, A. K. Rathore and D. Srinivasan, "Improved Modulation Strategy Using Dual Phase Shift Modulation for Active Commutated Current-Fed Dual Active Bridge," in IEEE Transactions on Power Electronics, vol. 33, no. 9, pp. 7359-7375, Sept. 2018.

[8] S. Samantara, B. Roy, A. Rout and R. Sharma, "Modeling and simulation of CUK converter with beta (B) MPPT for standalone PV system," Michael Faraday IET International Summit 2015, 2015.

[9] X. Li, H. Wen and C. Zhao, "Improved beta parameter based MPPT method in photovoltaic system," 2015 9th International Conference on Power Electronics and ECCE Asia (ICPE-ECCE Asia), 2015.

[10] X. Li, H. Wen, L. Jiang, W. Xiao, Y. Du and C. Zhao, "An Improved MPPT Method for PV System With Fast-Converging Speed and Zero Oscillation," in IEEE Transactions on Industry Applications, vol. 52, no. 6, pp. 5051-5064, Nov.-Dec. 2016.

[11] M. A. Elgendy, B. Zahawi, and D. Atkinson, "Operating characteristics of the p&o algorithm at high perturbation frequencies for standalone pv systems," IEEE Trans. Energy Convers., vol. 30, no. 1, pp. 189–198, Mar. 2015.

[12] X. Li, H. Wen, and C. Zhao, "Improved beta parameter based mppt method in photovoltaic system," in Proc. IEEE 9th Int. Power Electron. ECCE Asia Conf., Jun. 2015.

[13] B. Soreng, R. Garnayak and R. Pradhan, "A Synchronous Reference Frame based PLL Control for a Grid-Tied Photovoltaic System," 2017 International Conference on Current Trends in Computer, Electrical, Electronics and Communication (CTCEEC), 2017.

[14] Z. Alqarni, "Maximum Power Point Tracking for Solar Photovoltaic System using Synchronous Reference Frame Theory," 2021 IEEE 12th Annual Information Technology, Electronics and Mobile Communication Conference (IEMCON), 2021.

[15] C. A. Busada, S. G. Jorge and J. A. Solsona, "A Synchronous Reference Frame PI Current Controller With Dead Beat Response," in IEEE Transactions on Power Electronics, vol. 35, no. 3, pp. 3097-3105, March 2020.

[16] X. Quan and A. Q. Huang, "PI-Based Synchronous Reference Frame Frequency-Locked Loop," in IEEE Transactions on Industrial Electronics, vol. 68, no. 5, pp. 4547-4553, May 2021.

[17] Bhatti, A.R., Salam, Z., Bin Abdul Aziz, M.J., et al.: 'Electric vehicles charging using photovoltaic: status and technological review', Renew. Sust. Energy Rev., 2016.

[18] Morstyn, T., Momayyezan, M., Hredzak, B., et al. 'Distributed control for state-of-charge balancing between the modules of a reconfigurable battery energy storage system', IEEE Trans. Power Electron., 2016.

[19] Xue, L., Shen, Z., Boroyevich, D., et al.: 'Dual active bridge-based battery charger for plug-in hybrid electric vehicle with charging current containing low frequency ripple', IEEE Trans. Power Electron., 2015.

[20] Zhang, K., Shan, Z., Jatskevich, J.: 'Large- and small-signal average-value modeling of dual-active-bridge DC–DC converter considering power losses', IEEE Trans. Power Electron., 2017.

[21] S. Liu, D. Xin, L. Yang, J. Li and L. Wang, "A Hierarchical V2G/G2V Energy Management System for Electric-Drive-Reconstructed Onboard Converter," in IEEE Access, vol. 8, pp. 198201-198213, 2020.

[22] S. H. Hosseini, R. Ghazi and H. Heydari-Doostabad, "An Extendable Quadratic Bidirectional DC–DC Converter for V2G and G2V Applications," in IEEE Transactions on Industrial Electronics, vol. 68, no. 6, pp. 4859-4869, June 2021.

[23] H. Heydari-doostabad and T. O'Donnell, "A Wide-Range High-Voltage-Gain Bidirectional DC–DC Converter for V2G and G2V Hybrid EV Charger," in IEEE Transactions on Industrial Electronics, vol. 69, no. 5, pp. 4718-4729, May 2022.

[24] Aditya, Rachit Bansal, Akshit Goel, N.K. Jain and Uma Nangia (2022), Identifying and Mitigating the Barriers for Vehicle-to-Grid Adoption in India. IJEER 10(3), 447-453. DOI: 10.37391/IJEER.100307.

International Journal of
Electrical and Electronics Research (IJEER)
Research Article | Volume 11, Issue 1 | Pages 192-201 | e-ISSN: 2347-470X

[25] Himabindu Eluri, M. Gopichand Naik (2022), Energy Management System and Enhancement of Power Quality with Grid Integrated Micro-Grid using Fuzzy Logic Controller. IJEER 10(2), 256-263. DOI: 10.37391/IJEER.100234.

[26] Femy P. H., Jayakumar J. (2021), A Review on the Feasibility of Deployment of Renewable Energy Sources for Electric Vehicles under Smart Grid Environment. IJEER 9(3), 57-65. DOI: 10.37391/IJEER.0903061.

[27] Shaik Masum Basha and Dr. K. Nagaraju (2022), Controlling of Cascaded Voltage Source Two Level Inverter Based Grid Connected PV System by Using SVPWM and Quadratic Boost Converter. IJEER 10(3), 716-721. DOI: 10.37391/IJEER.100349.

AUTHOR(s) BIOGRAPHY

Ramesh Jatoth received his B.Tech degree in Electrical and Electronics Engineering and M.Tech in Power System from NIT calicut, Kerala, India, in 2008 to 2010 respectively. His research interests include Power Electronics, Power converters, Renewable energy sources with integrated electric vehicles. Presently he is pursuing Ph.D. in Osmania University, Hyderabad, India.

Prof. B. Mangu (Member, IEEE) he received the B.E. and M.E. degrees from the University College of Engineering, Osmania University, Hyderabad, India, in 2000 and 2005, and the Ph.D. degree with the Department of Electrical Engineering, IIT Bombay, Mumbai, India. He has been with the Department of Electrical Engineering, University College of Engineering, Osmania University, since 2001, where he is also a Professor. His current research interests include design of converters for integration of renewable sources.